Magnetic Mesoflowers: Synthesis, Assembly, and Magnetic Properties[†]

P. R. Sajanlal and T. Pradeep*

DST Unit on Nanoscience (DST UNS), Department of Chemistry and Sophisticated Analytical Instrument Facility, Indian Institute of Technology Madras, Chennai 600 036, India

Received: April 9, 2010; Revised Manuscript Received: June 18, 2010

An efficient method to introduce magnetic attributes to highly complex Au mesostructures by overlayer growth is demonstrated. The overlayer is nanostructured in all the cases investigated. A possible mechanism for the reduction of ions on the surface of Au mesoflowers and the consequent formation of hybrid mesoflowers is discussed. We studied the magnetic hysteresis behavior of Au/Ni, Au/Co, and Au/Pt/Ni mesoflowers at room temperature. Compared to the bulk metals, a decrease in saturation magnetization was observed in all the three hybrid magnetic mesoflowers, which may be due to the nanoscale structure. Assemblies of various magnetic mesoflowers extending over hundreds of micrometers on indium tin oxide (ITO) substrates have been made by magnetic field-induced self-assembly. Particles are assembled to form elongated chains, oriented parallel to the direction of the applied magnetic field.

Introduction

Synthesis of anisotropic magnetic nanoparticles with large surface areas received enormous attention not only due to their unusual physical and chemical properties but also due to wide range of applications in diverse areas such as high density data storage,[1] medical diagnosis,[2] catalysis,[3] ferrofluid technology,[4] contrast enhancement in magnetic resonance imaging,[5] and site-specific drugs delivery,[6] to mention a few. Since it is possible to tune the properties by introducing anisotropy into nanoparticles, enormous effort has been expended in developing anisotropic nanostructures such as rods, wires, flowers, etc.[7] Gold mesoflowers[8] (Au MFs) are a new category of anisotropic materials, having 5-fold symmetric multiple stems originating from the center giving a flower-like appearance to the object. They can be made in a range of sizes from 200 nm to 10 μm with high shape purity and in gram scale, by a seed-mediated growth process. A variety of aspects of these materials, such as near-infrared absorption, surface-enhanced Raman scattering (SERS), mechanism of growth, etc. have been examined.[8]

In view of making efficient and high-density memory storage devices, it is necessary to have patterned magnetic nanoparticle assemblies on selected substrates. Alignment of magnetic nanoparticles in a magnetic field is a facile technique for assembling nanoparticles into hierarchical assemblies. Magnetic fields have been used to make one- and two-dimensional assemblies of magnetic nanoparticles at the liquid−air interface and on solid substrates.[9] Cross junctions and T junctions of nanowire networks on unpatterned substrates and predefined lithographically patterned ferromagnetic electrodes, respectively, are also reported.[10] Patterning of magnetic nanoparticles on substrates has been achieved by the chemical adhesion between a substrate and magnetic nanoparticles with nonmagnetic coating.[11]

Although highly complex magnetic nanostructures have promising applications in diverse areas, synthesis of monodisperse materials in high yield with uniform shape is a major challenge. Most of the conventional, solution-based synthetic approaches yield anisotropic nanoparticles with wide size and shape distribution. An alternate way to overcome this limitation is to make an overcoating of desired magnetic materials over a complex nanostructure, which can be synthesized easily in high yield with monodispersity. Recently, we have demonstrated the incorporation of multiple attributes onto the meso/nanoflowers in the form of coating of various metals by a simple overgrowth mechanism.[12] Since gold is inefficient for the overcoating of magnetic materials such as nickel, platinum has been used as a sandwich for making nickel-coated magnetic gold nanoparticles.[13] In such cases, catalytic activity of Pt can be used for the growth of magnetic coating over the surface of Au nanoparticles.

In this paper, we demonstrate the magnetic functionalization of Au MFs by simple solution-based reduction of various metal ions such as Ni^{2+} and Co^{2+}, to form bimetallic MFs, such as Au/Ni and Au/Co, and trimetallic Au/Pt/Ni magnetic MFs by using the hydrazine hydrate-based reduction procedure. Even though the surface functionalization of Au nanoparticle with transition metals such as Ni, Co, and so forth is comparatively difficult than the other metals such as Pt, Ag, Pd, and so forth, we could successfully create a coating of these metals in a controlled and continuous fashion. Besides investigating their structure, we explored the magnetic properties of these hybrid MFs and made their long-range assemblies on ITO substrates by a magnetic field-induced self-assembly process.

Experimental Procedure

Materials. Tetrachloroauric acid trihydrate ($HAuCl_4 \cdot 3H_2O$), cetyltrimethylammonium bromide (CTAB), ascorbic acid, and $AgNO_3$ were purchased from CDH, India. $NiCl_2$, $CoCl_2$, and hydrazine hydrate were purchased from SD Fine Chemicals, India. Hexachloroplatinic acid ($H_2PtCl_6 \cdot 6H_2O$) was purchased from Sigma Aldrich. All chemicals were used as such without further purification. Triply distilled water was used throughout the experiments.

Synthesis of Gold Mesoflowers. This synthesis was performed as per our earlier report.[8] Briefly, 20 mL of CTAB (100 mM) was taken in a beaker and 335 μL of Au^{3+} (25 mM), 125

[†] Part of the special issue "Protected Metallic Clusters, Quantum Wells and Metallic Nanocrystal Molecules".

* To whom correspondence should be addressed. E-mail: pradeep@iitm.ac.in. Fax: + 91-44 2257-0545.

μL of AgNO$_3$ (10 mM), and 135 μL of ascorbic acid (100 mM) were added sequentially. To this solution, 2 mL of Au/oligoaniline nanoparticles[14] was added and the solution was maintained at 80 °C for 1 h. It was then allowed to cool to room temperature. After 1 h, the suspension was centrifuged at 3500 rpm for 4 min. The residue was washed with water three times to remove excess CTAB and other unwanted materials. The slight yellowish residue of Au MFs was redispersed in 20 mL of deionized water. The effective concentration of Au in the MF suspension is 0.418 mM, assuming that all the metal ions are reduced.

Synthesis of Au@Ni and Au@Co Mesoflowers. Bimetallic Au@Ni and Au@Co MFs were synthesized by a solution-based chemical reduction method. For that, 5 mL of Au MF suspension was taken in a sample bottle and sonicated well. The suspension was heated to 80 °C for 5 min. A solution containing 0.1 mL of 150 mM NiCl$_2$ or CoCl$_2$ in water was added into the above suspension. For making Au@Ni MFs, 0.5 mL of hydrazine hydrate, followed by 0.5 mL of 500 mM sodium hydroxide was added. In the case of synthesis of Au@Co MF, a mixture of 0.5 mL of 500 mM sodium hydroxide and 1 mL of hydrazine hydrate were added to the Au MF suspension. In both the cases, the temperature of the mixture was maintained at 80 °C. As the time goes, the color of the Au MFs changed to black. The resulting black magnetic MFs were separated with the help of a hand-held magnet and washed with absolute ethanol and triply distilled water in sequence. To increase the thickness of Ni coating, the amounts of NiCl$_2$ and hydrazine hydrate were increased to 0.3 and 1 mL, respectively. To increase the thickness of the Co coating, the amounts of Co^{2+} and hydrazine hydrate was increased to 0.3 and 2 mL, respectively.

Synthesis of Au/Pt/Ni Mesoflowers. For the synthesis of Au/Pt/Ni MFs, first we synthesize Au/Pt MFs using our earlier procedure.[12] Briefly, 5 mL of the as synthesized MFs was treated with 1 mL of 100 mM CTAB, 2 mL of 50 mM H$_2$PtCl$_6$, and 500 μL of ascorbic acid (100 mM). This was kept at room temperature for 5 h. After that, the suspension was centrifuged at 2000 rpm for 5 min. The black-colored residue was redispersed in 5 mL distilled water and centrifuged. This process was repeated 3 times to remove the unreacted ions and smaller Pt nanoparticles formed during this process. To the above suspension of Au/Pt MF, 0.3 mL of 150 mM NiCl$_2$ solution was added followed by the addition of 2 mL of hydrazine hydrate. The suspension was kept at room temperature for 5 h. The resultant black Au/Pt/Ni MF residue was washed with ethanol and water. In the absence of NaOH, a catalytic surface is necessary to get uniform coating on the Au MF. A thin Pt coating on Au MF surface can act as nuclei on which Ni could be catalytically reduced.[13]

Magnetic Field-Induced Assembly of Mesoflowers. To make an assembly of magnetic MFs, a suspension of purified MFs (Au/Ni or Au/Co) was drop-casted onto an ITO glass plate. When a permanent magnet (5000 G) was placed near to this ITO plate, these MFs self-assembled into an ensemble of elongated chains. We optimized the distance between the ITO plate and the magnet to get a long-range assembly. The MF suspension was then allowed to dry, while keeping the external magnetic field. The alignment was predominantly parallel to the applied magnetic field.

Instrumentation

Scanning electron microscopic (SEM) images and energy dispersive analysis of X-ray (EDAX) studies were done with a FEI QUANTA-200 SEM. Field-emission scanning electron microscopic (FESEM) measurements were carried out using an FEI Nova NanoSEM 600 instrument. For SEM measurements, samples were drop-casted onto an indium tin oxide (ITO)-coated conducting glass and air-dried. Transmission electron microscopy (TEM) was carried out using a JEOL 3011, 300 kV instrument with an ultrahigh-resolution (UHR) pole piece. The samples for TEM were prepared by dropping the suspension onto amorphous carbon films supported on a copper grid and dried in ambience. XPS measurements were done with Omicron ESCA Probe spectrometer with unmonochromatized Al Kα X-rays (hν = 1486.6 eV). The samples were spotted as drop-cast films on the sample stub and dried in a vacuum desiccator. X-ray flux was adjusted to reduce the beam-induced damage of the sample. The energy resolution of the spectrometer was set at 0.1 eV at a pass energy of 20 eV for typical measurements. Magnetic measurements were carried out with a vibrating sample magnetometer using a Physical Properties Measurement System (PPMS, Quantum Design, USA). X-ray diffraction (XRD) data were collected with a Shimadzu XD-D1 diffractometer using Cu Kα (λ = 1.54 Å) radiation. The samples were scanned in the 2θ range of 10−90°.

Results and Discussion

Hybrid magnetic MFs were synthesized as per the method explained in the experimental section. To begin with, Au MFs of definite morphology and structural attributes were synthesized. The MFs were characterized thoroughly by using SEM. The unique structural attributes of the gold MFs[8] such as large number of pentagonal stems with ridges along the edges were confirmed by SEM before the experiment (Figure 1A−C). The particles were of uniform size. MFs with all the characteristic features[8] were used for the subsequent experiments. We made magnetic shells of varying thicknesses by adjusting the concentration of Ni^{2+} and Co^{2+}. At lower concentrations, a thin coating of these metals were formed on the surface of the Au MF. Figure 1D,E shows large area SEM images of Au/Ni and Au/Co MFs, respectively. From these images it is clear that the bimetallic MFs had grossly the same shape as that of the parent materials.

From a detailed study of single Au/Ni and Au/Co MFs using SEM (Figure 2A,D), it was found that the structural attributes such as pentagonally symmetric stems and ridges along the edges almost disappeared after Ni or Co coating. The chemical composition of these bimetallic MFs was studied using EDAX. Figure 2 panels B and C are the Au Mα- and Ni Kα-based EDAX images, respectively, of the Au/Ni MF. EDAX data suggested that the ratio of weight percentage of Au and Ni in Au/Ni MF is ∼3:1 (see Supporting Information 1). The spatial extent of Au in the elemental image is smaller than that of Ni, implying an overlayer coating of Ni on the Au MF. Similarly, Figure 2E,F shows the Au Mα- and Co Kα-based EDAX images, respectively, of the Au/Co MF. In the case of Au/Co MFs, the weight percentage ratio between Au and Co was ∼5:1 (see Supporting Information 2). It was also noticed that surfaces of Au/Ni and Au/Co MFs were rough with tiny hairy projections on the surface.

One of the interesting factors we observed during the synthesis was the role of NaOH. In the case of Ni overcoating, the pH of the solution was found to be around 11. The bimetallic MF formation was almost unnoticed when the reaction was carried out in the absence of NaOH. In this case, smaller particles of Ni were formed in the suspension. This reveals the crucial role of NaOH in the reduction process of Ni on Au surfaces.[15] A possible mechanism of Ni overcoating on Au MF
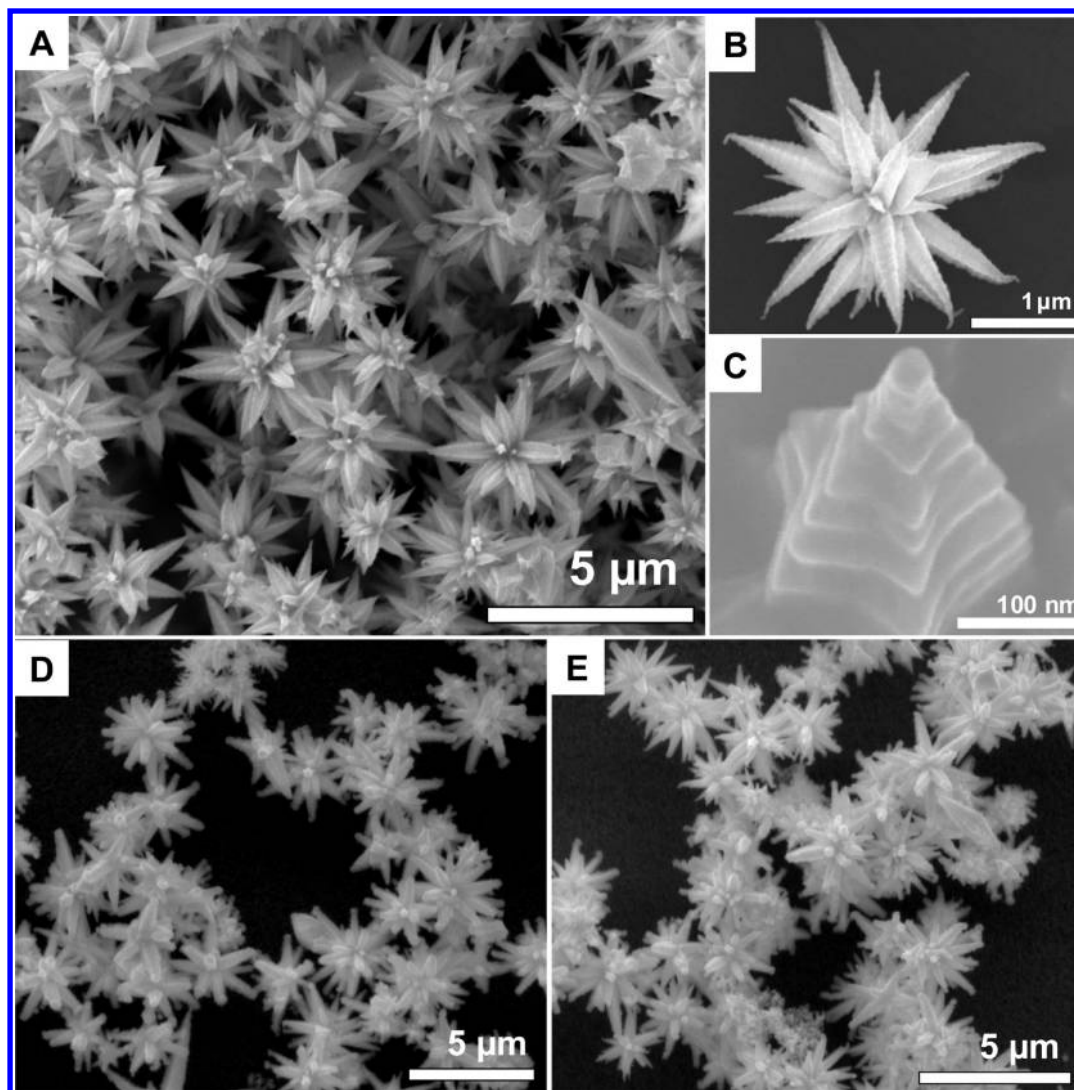
Figure 1. Large area SEM images of Au MFs (A) and a FESEM image of a single Au MF (B). The pentagonal symmetry of the stem is clearly visible in the top view of the stem shown in panel C. Large area SEM images of bimetallic Au/Ni (D) and Au/Co (E) MFs. In both cases, the amount of Ni and Co ions used during the synthesis was 0.1 mL (150 mM).

is as follows. Upon addition, Ni^{2+} forms a water-soluble complex with hydrazine hydrate.[16] After the subsequent addition of NaOH, the nickel-hydrazine complex gets converted into nickel hydroxide

$$[Ni(N_2H_4)n]Cl_2 + 2NaOH \rightarrow Ni(OH)_2 + nN_2H_4 + 2NaCl \tag{1}$$
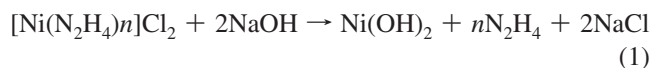
Subsequently, the nickel hydroxide undergoes reduction in presence of hydrazine hydrate to form black metallic Ni (eq 2)

$$2Ni(OH)_2 + N_2H_4 \rightarrow 2Ni + N_2 + 4H_2O \tag{2}$$

During this reaction, the Au MFs present inside the suspension may act as the nucleation centers and Ni reduction may happen on the surface of Au MF. Because of the catalytic activity of as formed Ni, hydrazine hydrate decomposes[16] as

$$N_2H_4 \rightarrow N_2 + 2H_2 \tag{3}$$

$$3N_2H_4 \rightarrow N_2 + 4NH_3 \tag{4}$$
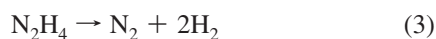
Due to this reason, we used excess hydrazine hydrate for the reduction. Also, we noticed that Co overcoating will not happen in the absence of NaOH. In both the cases, individual Co or Ni nanoparticles were absent in the suspension.

In order to increase the loading of the magnetic shell over the Au MF, we increased the amount of Ni and Co (0.3 mL, 150 mM). At this condition, thick coatings of Ni and Co shells were formed on the parent MFs. The resemblance to the parent MFs almost disappeared at this stage. At the same time, they maintained flower-like geometry. Figure 3 shows the single particle SEM images and corresponding EDAX images of the Au/Ni and Au/Co MFs. Au to Ni weight ratio of the resultant Au/Ni MF was approximately 1:3. EDAX image also reveals the presence of oxygen on the surface of Au/Ni MF (see Supporting Information 1). Even though it is expected that the presence of oxygen on the ITO substrate can interfere with the measurements, the EDAX image clearly shows that a considerable amount of oxygen is present on the surface of Au/Ni MF, probably due to the oxidation of surface Ni (see Supporting Information 1).
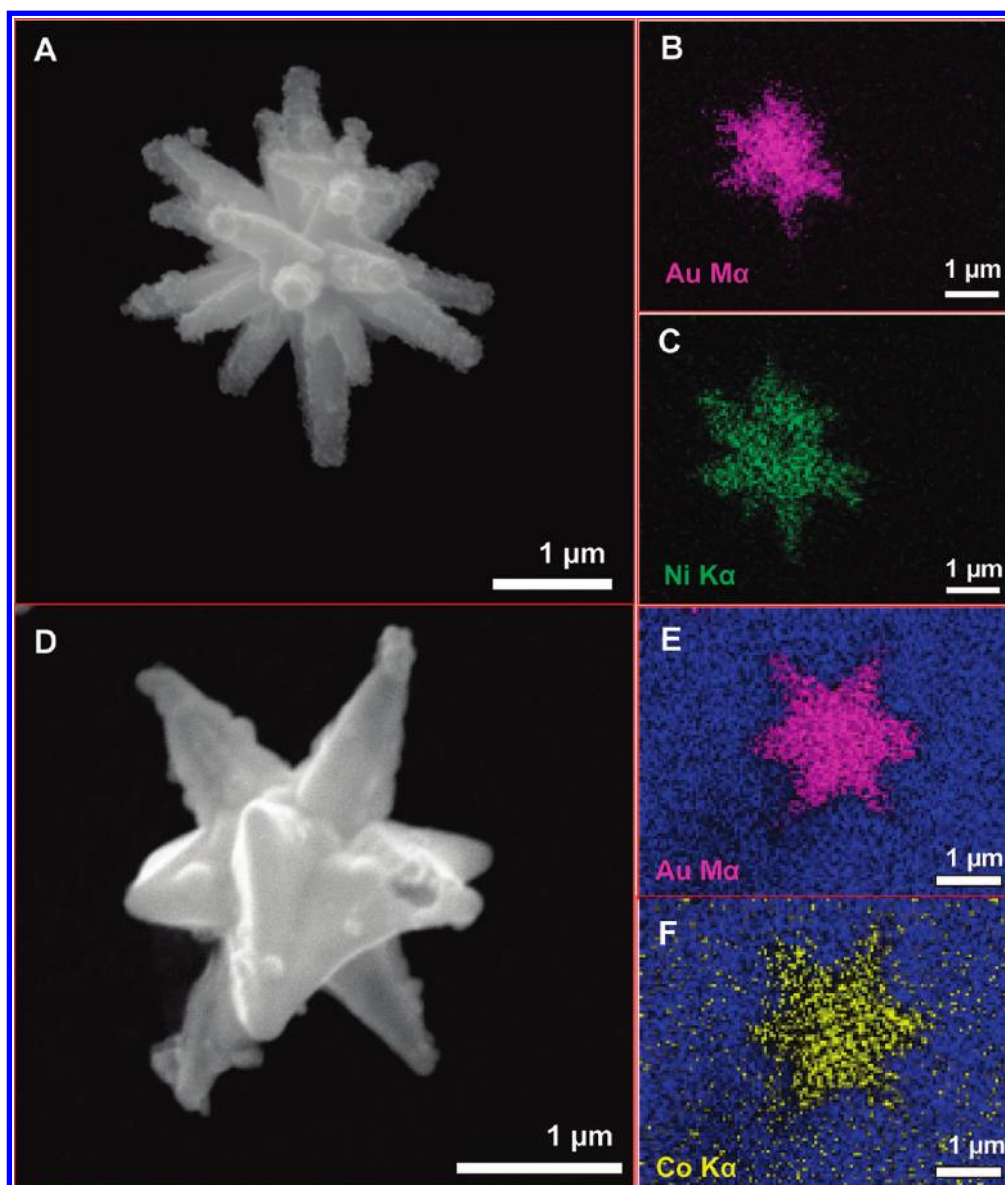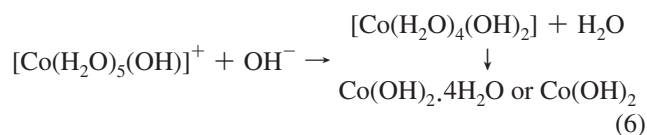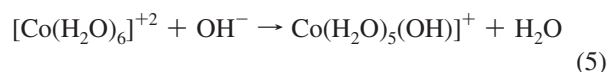
Figure 2. (A) SEM image of a single Au/Ni MF. (B,C) Corresponding Au Mα- and Ni Kα-based EDAX images collected from the sample shown in panel A. (D) Single particle SEM image of Au/Co MF. A Au Mα- and Co Kα-based EDAX image of Au/Co MF (D) is shown in panels E,F, respectively. The amount of Ni and Co ions used during the synthesis was 0.1 mL (150 mM).

As Figure 3A shows that high loading of Ni drastically changed the morphology of Au MF to a large extent and the surface of the bimetallic Au/Ni MF appeared to have a hairy morphology. Almost similar morphology was observed in the case of Au/Co MF (Figure 3D). Large area SEM images of Au/Ni and Au/Co MFs at this condition are given in Supporting Information 3. It was found that a sizable amount of Au got replaced by Co in Au/Co MF, as evidenced from the EDAX image (Figure 3E, F) and quantification data (see Supporting Information 2). The amount of Co was nearly 8 times greater than the weight percentage of Au at this condition. The presence of oxygen on Au/Co MF surface was also confirmed from the EDAX data.

The mechanism of cobalt overcoating on the Au MF surface can be explained as follows. It is known that cobalt ions can exist in the form of hexaaquacobalt(II) complex in water.[17] Sodium hydroxide reacts with this complex to form a neutral cobalt hydroxide complex (eqs 5 and 6), which is insoluble in water and appeared as a turbidity. Simultaneously, hydrazine hydrate reduces Co^{2+} to Co^0 (eq 7)

$$[Co(H_2O)_6]^{+2} + OH^- \rightarrow [Co(H_2O)_5(OH)]^+ + H_2O \tag{5}$$

$$[Co(H_2O)_5(OH)]^+ + OH^- \rightarrow \begin{array}{c} [Co(H_2O)_4(OH)_2] + H_2O \\ \downarrow \\ Co(OH)_2 \cdot 4H_2O \text{ or } Co(OH)_2 \end{array} \tag{6}$$

$$2Co(OH_2) + N_2H_4 \rightarrow 2Co + N_2 + 4H_2O \tag{7}$$

The absence of individual Co nanoparticles in the suspension reveals that Au MFs act as nucleation centers for the reduction of Co ions. This results in Co deposition at the Au MF surface.

A detailed analysis of Au/Ni and Au/Co MFs was done using TEM (Figure 4). Tiny hair-like projections on the surfaces of the MFs were clearly seen in the TEM images (Figure 4A,C). Lattice resolved images of both Au/Ni and Au/Co MFs (Figure 4B,D) show that the directions of the lattice fringes are different at various regions within a single MF. The observed lattice
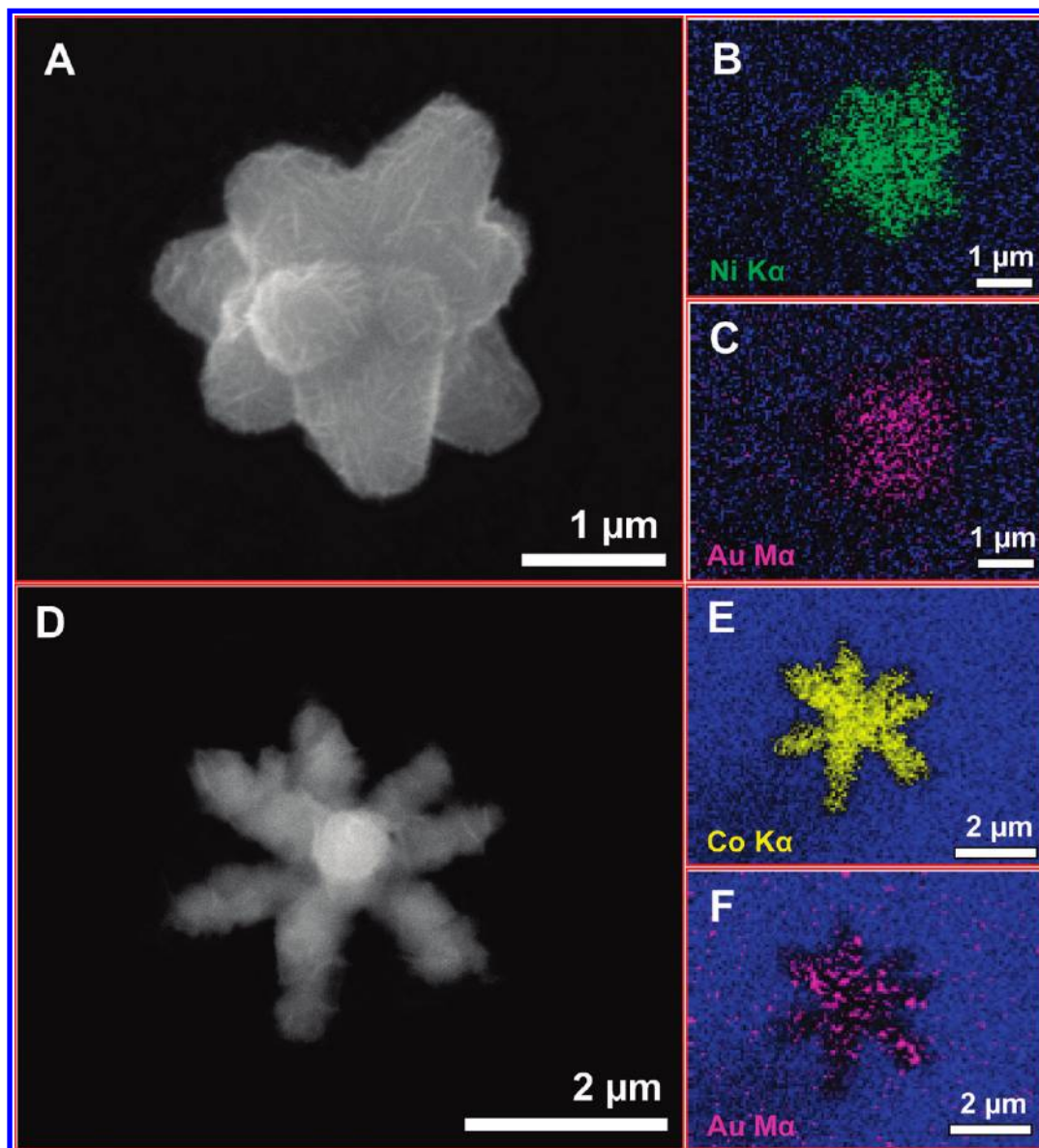
Magnetic Mesoflowers

J. Phys. Chem. C, Vol. 114, No. 38, 2010 **16055**

Figure 3. (A) SEM image of a single Au/Ni MF. (B,C) Corresponding Ni Kα- and Au Mα-based EDAX images collected from the sample shown in panel A. (D) Single particle SEM image of Au/Co MF. Co Kα- and Au Mα-based EDAX image of Au/Co MF (D) is shown in panels E and F, respectively. The amount of Ni and Co ions used during the synthesis was 0.3 mL (150 mM).

spacing is 2.02 Å in Au/Ni MF (Figure 4B) and can be indexed to the (111) planes of face-centered cubic (fcc) Ni, coated on the Au surface. The *d*-spacing of ∼2.39 Å can be due to the (111) lattice plane of fcc NiO, which was formed by the oxidation of the Ni surface. In the case of Au/Co MFs, the measured lattice spacing of 2.01 Å can be indexed to the (111) plane of fcc cobalt. The *d*-spacing 2.44 Å found in the lattice-resolved image may be assigned to the (111) planes of the CoO. Random orientation and multiple twinning of the lattice planes observed in the magnified TEM images reveals the polycrys-talline nature of the Ni and Co coating on the surface of Au MFs. Single particle TEM images of Au/Ni and Au/Co MFs are given in Supporting Information 4.

To incorporate more functionality as in the form of a new metal into the MF, an experiment was also conducted to make trimetallic MFs comprised of Au, Pt, and Ni. Here, the catalytic activity of Pt is made use of, instead of NaOH, to make a coating of Ni on the surface of Au MF. For that, first we made a thin coating of Pt on the gold MF using our earlier report.[12] Subsequently, deposition of Ni was carried out in the presence

of hydrazine hydrate without the aid of NaOH. Figure 5A,B shows the FESEM images of a single Au/Pt/Ni MF and an expanded image of its single stem, respectively. The amount of Ni deposited was less in this case. Elemental distribution in the Au/Pt/Ni MF was confirmed from the EDAX image (Figure 5C−E). EDAX spectrum and quantification data of Au/Pt/Ni MF are shown in Supporting Information 5. The morphology was almost similar as in the case of the parent MF. Magnified FESEM images show the gradual transformation of the surface texture as the growth of Pt and Ni occurred on the surface of the Au MF (Figure 6). As evidenced from the images, surface of the Au MF got roughened after the deposition of Pt. Upon Ni coating onto the Au/Pt surface, the smoothness and uniform surface structure got disrupted. We have observed that the surface of the Au/Pt MF became corrugated after the deposition of Ni. At the same time, stems with scale-like appearance and ridges along the edges were almost retained in this trimetallic MF as seen in the magnified FESEM image (Figure 5B).

The catalytic activity of Pt on Ni reduction was established by Liz-Marzán et al.[13b] Pt can be reduced easier than nickel
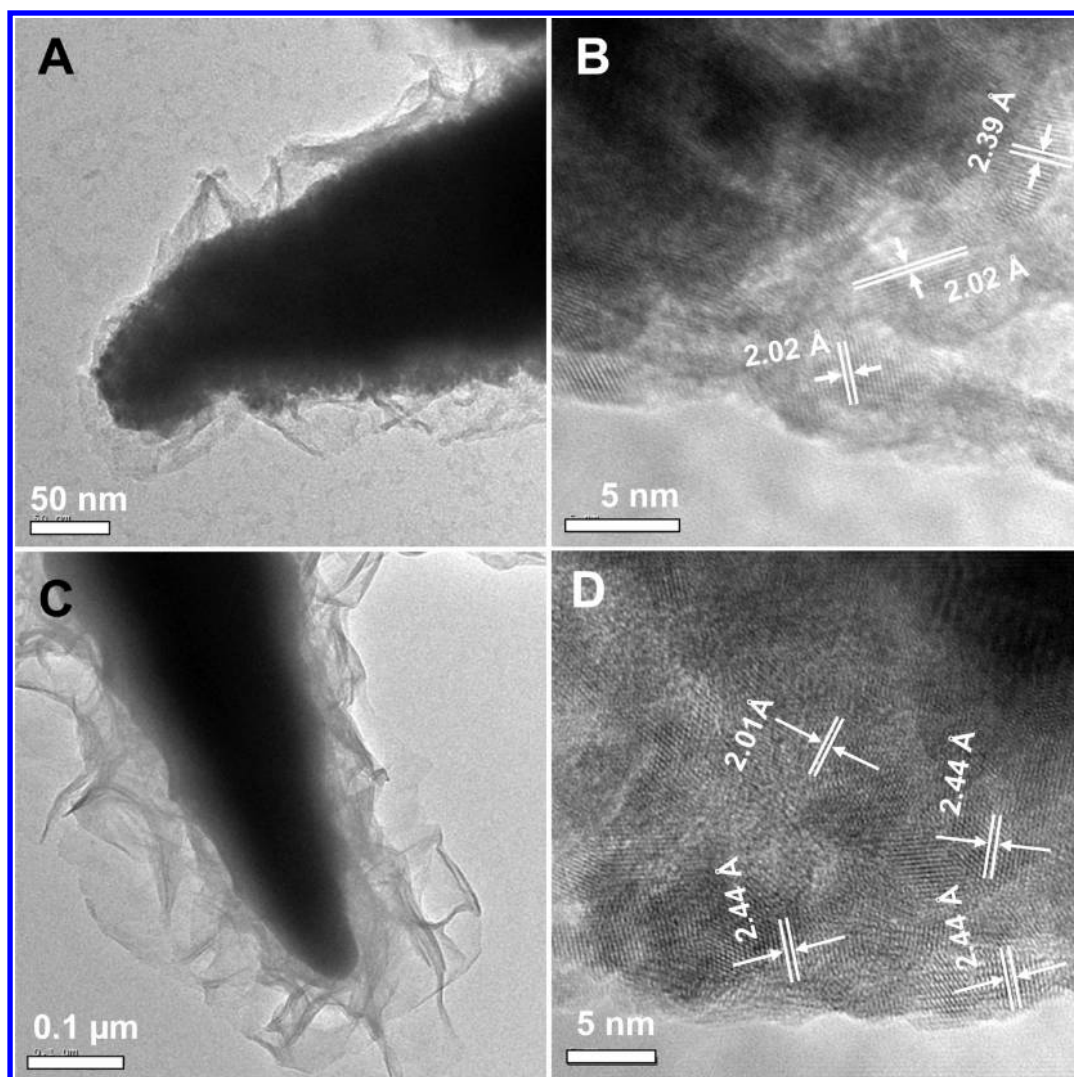
Figure 4. TEM images of the tip of the Au/Ni (A) and Au/Co (C) MFs. (B,D) Lattice-resolved images collected from the tip of the Au/Ni and Au/Co MFs, respectively. The amount of Ni and Co ions used during the synthesis was 0.1 (150 mM) and 0.3 mL (150 mM), respectively.

because of its higher reduction potential. The catalytic role of platinum seems to be related to the ease of decomposition of hydrazine on small nanoparticles. After the addition to the Ni^{2+} solution, hydrazine can partially undergo complexation with Ni^{2+}. The catalytic decomposition of noncomplexed hydrazine on the surface of platinum creates a charged metallic surface, where the Ni^{2+} complexes can be easily reduced to Ni^{0}.[13b]

To study the chemical composition, XPS spectra of all three hybrid MFs were analyzed. Figure 7A shows the wide scan XPS spectra of Au/Ni, Au/Co, and Au/Pt/Ni MFs. The enlarged XPS spectra in the Au 4f region of Au/Co, and Au/Ni MFs show the presence of Au $4f_{7/2}$ and Au $4f_{5/2}$ peaks at ~84.0 and ~87.7 eV, respectively, confirming that gold is existing in its metallic form. At the same time, we could not find the signature of Au in Au/Pt/Ni MFs (Figure 7F) since Au was buried under the Pt and Ni overlayers. This suggests that the overlayer thickness is larger than the mean free path and that the coating is complete and no free surface of Au MF is exposed. In the enlarged spectrum of Co 2p region in Au/Co MFs (Figure 7C), the peaks at ~778.5 and 793.8 eV can be attributed to metallic Co, whereas the peaks at ~782.6 and ~785.3 eV can be assigned to the Co^{2+}. This implies the possible coexistence of Co^{0} and Co^{2+} on the surface of the Au/Co MFs. The satellite features found in the high binding energy side of the $2p_{3/2}$ and $2p_{1/2}$ lines are characteristics of high spin Co^{2+}.[18] The O 1s spectrum of

Au/Co MFs (see Supporting Information 6) shows multiple peaks, which is indicative of the existence of various oxygen species at the MF surface. The peak observed at ~531.8 eV is considered to be due to the oxygen from CoO, whereas the peak found at the higher binding energy side (~535.5 eV) can be from the oxygen in oxyhydroxides. Oxygen from hydroxides and oxyhydroxides usually appears in the higher binding energy side compared to the oxide ions.[19] Enlarged scan of Ni 2p of Au/Ni MFs showed $2p_{3/2}$ at ~855.4 eV and $2p_{1/2}$ at ~873.1 eV (Figure 7E). A shift in the Ni 2P peaks of Au/Ni MFs toward the higher binding energy side compared to Ni^{0} (852.6 eV) reveals the possible existence of Ni^{2+} ions in the form of NiO coating on the surface of the Au/Ni MFs. The high-binding energy satellites confirm the divalent state.[20] The low-binding energy peak at 852.2 eV is attributed to the characteristic feature of Ni^{0}.[20c,d] The O 1s peak found at 531.0 eV (see Supporting Information 6) again confirms the presence of O^{2-}. In the enlarged spectrum of Pt 4f region of Au/Pt/Ni MFs (Figure 7H), the peaks observed at 70.9 and 74.3 eV correspond to Pt $4f_{7/2}$ and Pt $4f_{5/2}$. The $2p_{3/2}$ and $2p_{1/2}$ peaks of Ni, found at 855.4 and 873.1 eV, respectively (Figure 7G) support the oxide coating on the surface as in the case of Au/Ni MFs.[20] The satellite peaks associated with Ni 2p are also due to this.[20] Since the amount of Ni deposited in Au/Pt/Ni MFs was very less, the Ni^{0} feature
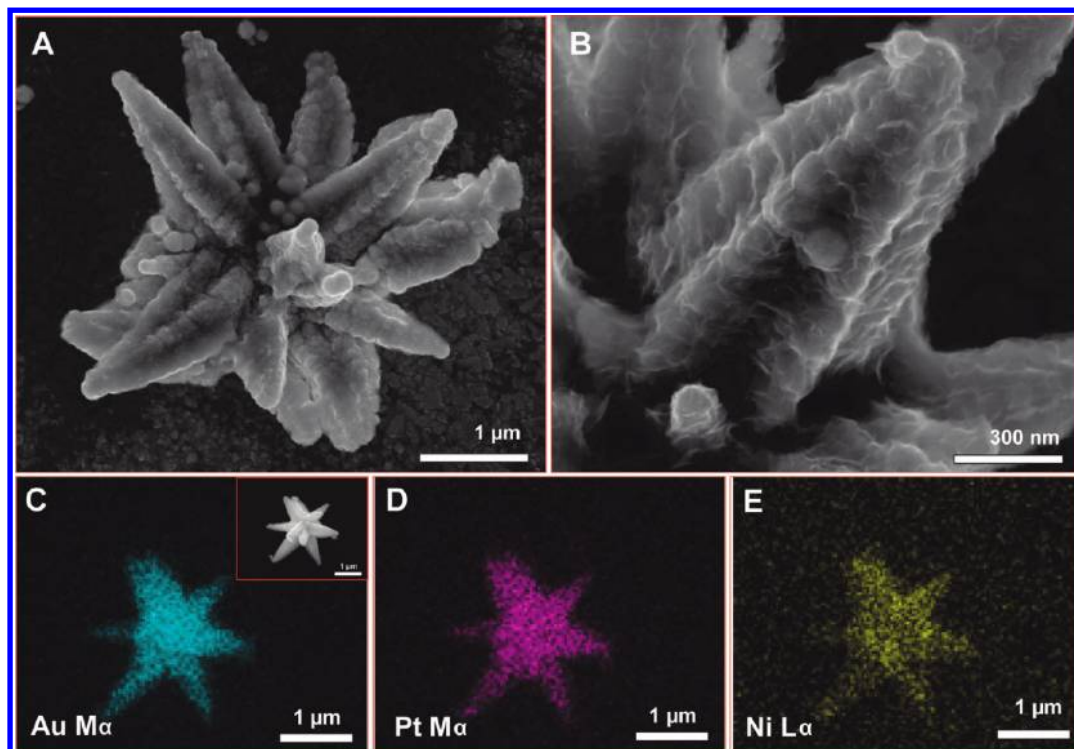
Figure 5. (A,B) The FESEM images of a single Au/Pt/Ni MF and an enlarged view of its stem, respectively. (C−E) The EDAX images of Au/Pt/Ni MF shown in the inset of panel C.
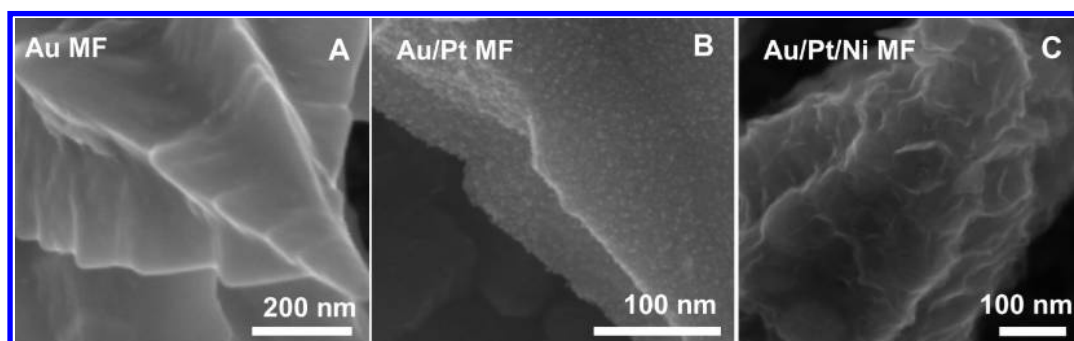

Figure 6. Magnified FESEM images of the stems of different MFs. (A) Au MF, (B) Au/Pt, and (C) Au/Pt/Ni MFs.
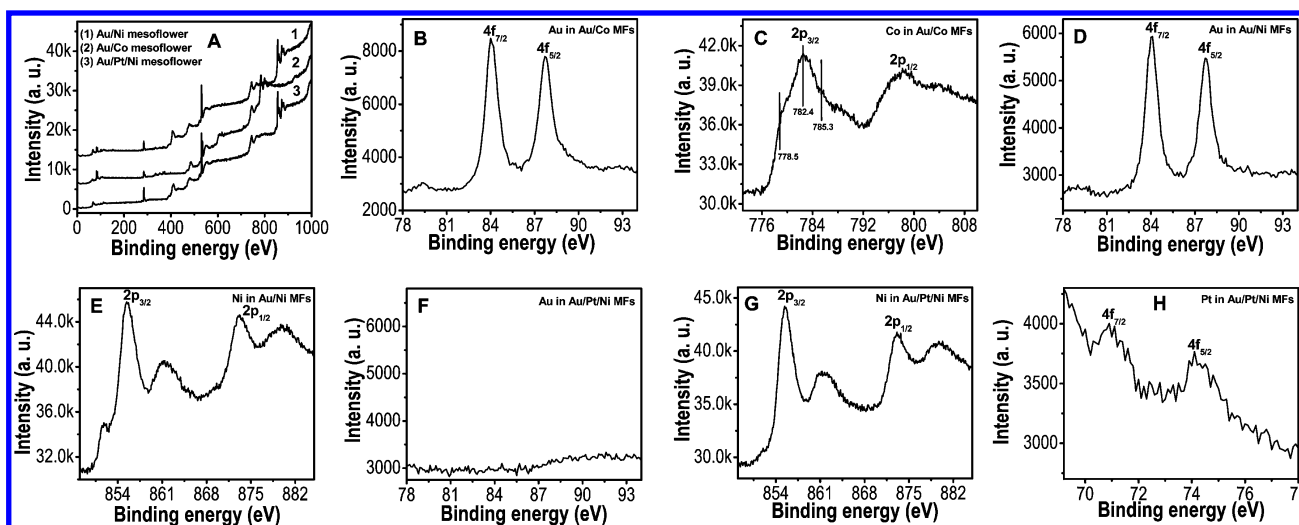

Figure 7. (A) Wide scan XPS spectra of Au/Ni, Au/Co, and Au/Pt/Ni MFs. (B,D,F) The Au 4f region of Au/Co, Au/Ni, and Au/Pt/Ni MFs, respectively. (C) XPS spectrum in the 2p region of Co in Au/Co MFs. (E,G) are the Ni 2p region of Au/Ni and Au/Pt/Ni MFs, respectively. (H) Pt 4f region of Au/Pt/Ni MFs.

at 852.2 eV was weak. The O 1s peak was found at 531.0 eV here as well (see Supporting Information 6).

Additionally, the presence of such coatings on the mesoflower surface was confirmed by the X-ray diffraction (XRD) analysis
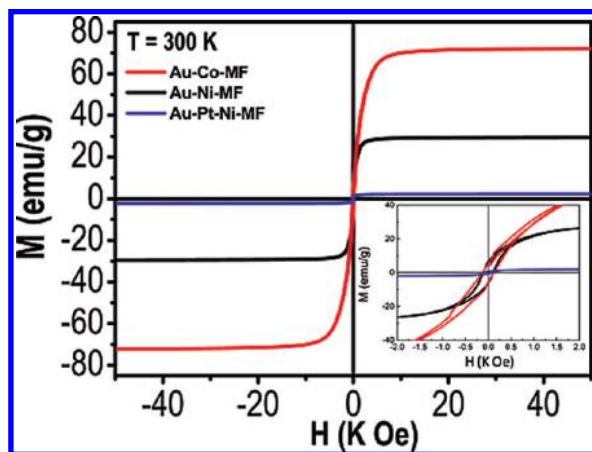
Figure 8. Magnetic hysteresis loops (M/H) of various magnetic MFs at 300 K. The inset shows the low-field part of the hysteresis loops. The amount of Ni and Co ions used during the synthesis was 0.3 mL (150 mM).

(see Supporting Information 7). For the XRD analysis, Au/Ni and Au/Co MFs were synthesized using 0.1 mL (150 mM) of Ni and Co ions, respectively. In the case of Au/Ni MFs, we found distinct diffraction features of Au and Ni; they were all in fcc (the ratio of weight percentage of Au and Ni in Au/Ni MF was ∼3:1). The features due to Co in Au/Co MFs were weak, since the amount of Co in the Au/Co MFs was much less (the weight percentage ratio between Au and Co was ∼5:1). Similarly, the characteristic features Au, Pt, and Ni were present in the XRD pattern of Au/Pt/Ni MFs. Characteristic XRD patterns of individual metals in various hybrid magnetic MFs show that the formation of alloys upon overgrowth is unlikely. Peaks due to oxides of Co and Ni were not prominent as they exist only as thin layers, although they are shown in XPS analysis.

We confirmed the ferromagnetic properties of Au/Ni, Au/Co, and Au/Pt/Ni MFs by measuring their hysteresis loops (M-H) at room temperature (300 K), as illustrated in Figure 8 (the magnetization shown in figure is for the entire sample, composed of all the elements). The presence of a nonzero coercivity and a nonzero remanence (inset of Figure 8) indicate the ferromagnetic behavior of these MFs. Among the three hybrid MFs, Au/Co MF showed a maximum saturation magnetization of 70.5 emu g^{-1}, which is much lower than that for the reported bulk Co metal (168.0 emu g^{-1}).[21] Even after correcting for the masses of Au, C, and O in the MF using the EDAX percentage, the magnetism appears to be low (∼91 emu/g), indicating the nanoscale effect. As seen in TEM, the constituent particles are much smaller in size.

In the case of Au/Ni and Au/Pt/Ni MFs, a substantial decrease was observed in the saturation magnetization compared to bulk Ni (55.0 emu g^{-1}).[22] Although their morphologies are similar, Au/Pt/Ni showed a lower saturation magnetization of 2.1 emu g^{-1} compared to that of Au/Ni MF (29.3 emu g^{-1}). A decrease in saturation magnetization in nanoparticles compared to the bulk metals is expected possibly due to various reasons such as existence of impurities,[23] surface antiferromagnetic oxides,[23] and surface spin disorder.[24]

Self-assembly and self-orientation of magnetic nanoparticles are very important for many applications. We could make a micrometer long assembly of bimtallic MFs on an ITO substrate by a simple method. We found that the magnetic MFs self-orient in such a way to form an ensemble of elongated chains in presence of an external magnetic field. The MFs were predominantly aligned parallel to the applied magnetic field. Figure 9A,E shows large area SEM images of assemblies of Au/Ni, and Au/Co MFs on ITO substrates, respectively. It was noticed that the long self-assembled chains are almost parallel to each other. SEM images of a single strand of Au/Ni (Figure 9B) and Au/Co MFs (Figure 9F) and their corresponding EDAX images are also given in Figure 9.

The distance between the ITO substrate and the magnet is found to play an important role in the assembly of the MFs. A long-range assembly with an average length of ∼50 μM was
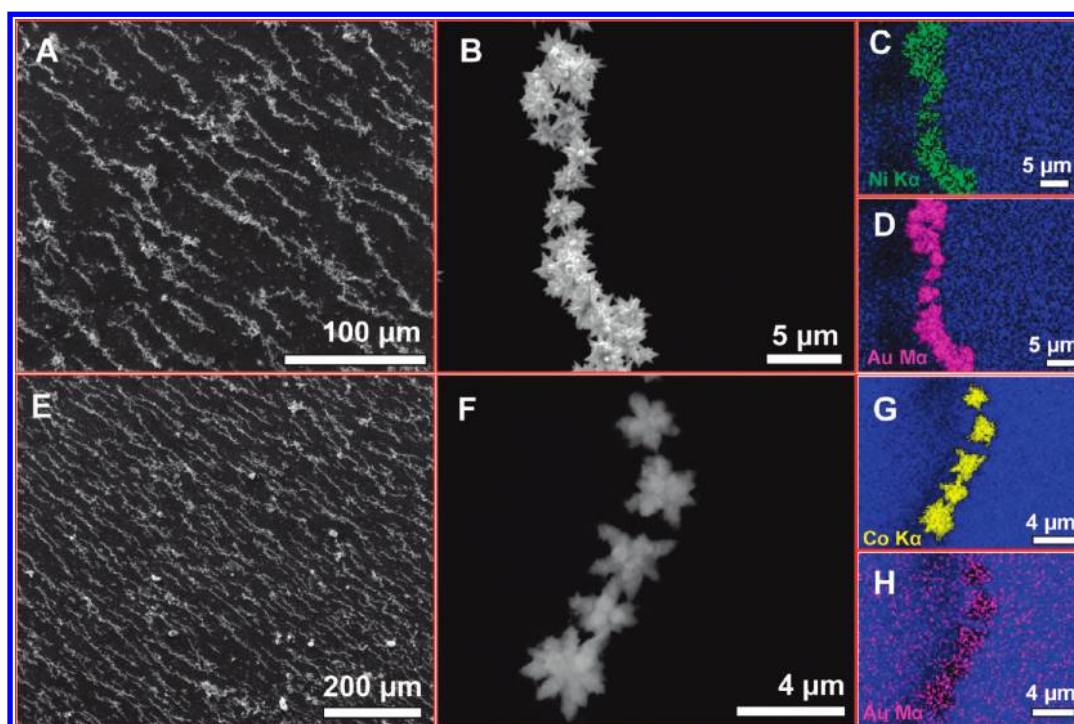

Figure 9. (A,E) SEM images showing the long-range, magnetic field-induced assembly of Au/Ni and Au/Co MFs, respectively. (B,F) Single strands of Au/Ni and Au/Co MF, respectively. Corresponding elemental maps are also given.

Magnetic Mesoflowers

J. Phys. Chem. C, Vol. 114, No. 38, 2010 **16059**

observed when the distance was maintained to be 2 cm. SEM images of individual chains are given in Supporting Information 8. It was noticed that all the MF were not part of the assembly. Alignment was seen over 1.5–2.5 cm. As the distance between the magnet and ITO substrate containing MFs was reduced to 1 cm, we found a random alignment of the MFs and they started aggregating at the end of the ITO plate, pointing toward the magnet. We did not see any alignment when the distance was above 3 cm. In the case of Au/Pt/Ni MF, the extent of alignment was not as good as in the other two MFs. The arrangement was almost random, as observable in the SEM image (see Supporting Information 9).

Since a long-range self-assembly of magnetic nanomaterials is a complex process, it can be influenced by various factors. In the presence of an external magnetic field, each MF can virtually act as a simple magnet. The magnetic moment of each particle can couple with the applied field. A dipole–dipole attraction between the particles may induce their assembly. Other factors such as electronic polarization interactions, thermal and kinetic effects, the properties of the media in which the particles are aligned, etc. may also influence the long-range assembly of these particles.[25] As the dipole–dipole interactions quadratically increase with the particle volume, larger particles may be expected to form long-range chain-like assemblies.[26] Even though there are numerous experimental and theoretical studies on the field-induced self-organization and aggregation of magnetic particles, an exact mechanism of this process is lacking in the literature.[9a,27]

Conclusions

We demonstrated a method to incorporate magnetic attributes to highly anisotropic Au MFs by the chemical reduction route. Various parameters responsible for the deposition of magnetic materials onto the MF were studied. We studied the magnetic hysterisis (M-H) of Au/Ni, Au/Co, and Au/Pt/Ni MFs at room temperature. A decrease in saturation magnetization was observed in all three hybrid MFs, possibly due to the nanoscale dimension of the materials. We also demonstrated a simple method to make long-range assemblies of various magnetic MFs on an ITO substrate via a magnetic field-induced self-assembly process. The particles were assembled into an elongated chain with a predominant orientation parallel to the direction of the applied field. Since it is possible to make nanoflowers of less than 100 nm using our procedure, these hybrid MFs may be used as good candidates in biological applications such as cancer cell treatment and site-specific drug delivery, especially in conjunction with other properties of MFs such as NIR absorption and Raman enhancement.[8]

Supporting Information Available: EDAX and quantification data of Ag/Ni, Au/Co, and Au/Pt/Ni MFs, large area SEM images of various magnetic MFs, TEM images of single Au/Ni and Au/Co MFs, XPS spectra showing O 1s in various MFs, XRD of various mesoflowers, and SEM images of the assembly of various MFs. This material is available free of charge via the Internet at http://pubs.acs.org.

References and Notes

(1) (a) Murray, C. B.; Kagan, C. R.; Bawendi, M. G. *Science* **1995**, *270*, 1335–1338. (b) Zeng, H.; Li, J.; Wang, Z. L.; Liu, J. P.; Sun, S. *Nature* **2002**, *420*, 395. (c) Shevchenko, E. V.; Talapin, D. V.; Rogach, A. L.; Kornowski, A.; Haase, M.; Weller, H. *J. Am. Chem. Soc.* **2002**, *124*, 12480.

(2) (a) Sun, S. H. *Adv. Mater.* **2006**, *18*, 393–403. (b) Gu, H.; Ho, P.-L.; Tsang, K. W. T.; Wang, L.; Xu, B. *J. Am. Chem. Soc.* **2003**, *125*, 15702. (c) Gu, H.; Zheng, R.; Zhang, X.; Xu, B. *J. Am. Chem. Soc.* **2004**, *126*, 5664.

(3) Stevens, P. D.; Fan, J.; Gardimalla, H. M. R; Yen, M.; Gao, Y. *Org. Lett.* **2005**, *7*, 2085.

(4) Raj, K.; Moskowitz, R.; Casciari, R. *J. Magn. Magn. Mater* **1995**, *149*, 174.

(5) Mitchell, D. G. *J. Magn. Reson. Imaging* **1997**, *7*, 1–5.

(6) Gupta, P. K.; Hung, C. T. *Life Sci.* **1989**, *44*, 175–186.

(7) (a) Zhang, Y.-J.; Zhang, Y.; Wang, Z.-H.; Li, D.; Cui, T.-Y.; Liu, W.; Zhang, Z.-D. *Eur. J. Inorg. Chem.* **2008**, 2733–2738. (b) Dumestre, F.; Chaudret, B.; Amiens, C.; Respaud, M.; Fejes, P.; Renaud, P.; Zurcher, P. *Angew. Chem., Int. Ed.* **2003**, *42*, 5213–5216.

(8) Sajanlal, P. R.; Pradeep, T. *Nano Res.* **2009**, *2*, 306.

(9) (a) Cheng, G.; Romero, D.; Fraser, G. T.; Walker, A. R. H. *Langmuir* **2005**, *21*, 12055. (b) Grzybowski, B. A.; Stone, H. A.; Whitesides, G. M. *Nature* **2000**, *405*, 1033–1036. (c) Wiedwald, U.; Spasova, M.; Farle, M.; Hilgendorff, M.; Giersig, M. *J. Vac. Sci. Technol., A* **2001**, *19*, 1773. (e) Petit, C.; Russier, V.; Pileni, M. P. *J. Phys. Chem. B* **2003**, *107*, 10333. (f) Sahoo, Y.; Cheon, M.; Wang, S.; Luo, H.; Furlani, E. P.; Prasad, P. N. *J. Phys. Chem. B* **2004**, *108*, 3380. (d) Tripp, S. L.; Pusztay, S. V.; Ribbe, A. E.; Wei, A. *J. Am. Chem. Soc.* **2002**, *124*, 7914.

(10) Hangarter, C. M.; Rheem, Y.; Yoo, B.; Yang, E.-H.; Myung, N. V. *Nanotechnology* **2007**, *18*, 205305.

(11) Seip, C. T.; O'Connor, C. J. *Nanostruct. Mater.* **1999**, *12*, 183.

(12) Sajanlal, P. R.; Pradeep, T. *Langmuir* **2010**, *26*, 8901.

(13) (a) Farrell, R. D.; Majetich, S.; Wilcoxon, J. *J. Phys. Chem. B* **2003**, *107*, 11022. (b) Grzelczak, M.; Rodríguez-González, B.; Pérez-Juste, J.; Liz-Marzán, L. M. *Adv. Mater.* **2007**, *19*, 2262.

(14) Sajanlal, P. R.; Sreeprasad, T. S.; Nair, A. S.; Pradeep, T. *Langmuir* **2008**, *24*, 4607.

(15) (a) Wu, S.-H.; Chen, D.-H. *J. Colloid Interface Sci.* **2003**, *259*, 282–286. (b) Hinotsu, T.; Jeyadevan, B.; Chinnasamy, C. N.; Shinoda, K.; Tohji, K. *J. Appl. Phys.* **2004**, *95*, 7477.

(16) Huang, G.-Y.; Xu, S.-M.; Xu, G.; Li, L.-Y.; Zhang, L.-F. *Trans. Nonferrous Metal Soc.* **2009**, *19*, 389–393.

(17) Shojaee, K. ; Edrissi, M.; Izadi. H. *J. Nanopart. Res.* **2010**, *12*, 1439.

(18) Jeong, B.-S.; Heo, Y. W.; Norton, D. P.; Kelly, J. G.; Rairigh, R.; Hebard, A. F.; Budai, J. D.; Park, Y. D. *Appl. Phys. Lett.* **2004**, *84*, 2608–2610.

(19) Stoch, J.; Gablankowska-Kukucz, J. *Surf. Interface Anal.* **1991**, *17*, 165.

(20) (a) Carley, A. F.; Jackson, S. D.; O'Shea, J. N.; Roberts, M. W. *Phys. Chem. Chem. Phys.* **2001**, *3*, 274. (b) Bokare, A. D.; Chikate, R. C.; Rode, C. V.; Paknikar, K. M. *Environ. Sci. Technol.* **2007**, *41*, 7437. (c) Sharma, S. K.; Zaporojtchenko, V.; Zekonyte, J.; Buettner, J.; Deki, S.; Faupel, F. *J. Mater. Sci.* **2004**, *39*, 6291. (d) Luo, P. F.; Kuwana, T.; Paul, D. K.; Sherwood, P. M. A. *Anal. Chem.* **1996**, *68*, 3330.

(21) Xie, Q.; Qian, Y. T.; Zhang, S. Y.; Fu, S. Q.; Yu, W. C. *Eur. J. Inorg. Chem.* **2006**, *37*, 2454–2459.

(22) Sun, X. C.; Dong, X. L. *Mater. Res. Bull.* **2002**, *37*, 991–1004.

(23) Zhang, L.; Manthiram, A. *Phys. Rev. B* **1996**, *54*, 3462–3467.

(24) Lin, D.; Nunes, A. C.; Majkrzak, C. F.; Berkowitz, A. E. *J. Magn. Magn. Mater.* **1995**, *145*, 343–348.

(25) Sahoo, Y.; Cheon, M.; Wang, S.; Luo, H.; Furlani, E. P.; Prasad, P. N. *J. Phys. Chem. B* **2004**, *108*, 3380–3383.

(26) Neto, C.; Bonini, M.; Baglioni, P. *Colloid Surf., A* **2005**, *269*, 96–100.

(27) (a) Ahniyaz, A.; Sakamoto, Y.; Bergstrom, L. *Proc. Natl. Acad. Sci. U.S.A.* **2007**, *104*, 17570–17574. (b) Ytreberg, F. M.; McKay, S. R. *Phys. Rev. E* **2000**, *61*, 4107. (c) Terheiden, A.; Dmitrieva, O.; Acet, M.; Mayer, C. *Chem. Phys. Lett.* **2006**, *431*, 113.